Towards More Accurate Matching of Contactless Palmprint Images under Less Constrained Environments

Ajay Kumar
Department of Computing, The Hong Kong Polytechnic University, Hung Hom, Hong Kong

Abstract: *Contactless personal identification using biometrics characteristics brings multifaceted advantages with improved hygiene, user security and the convenience. Such imaging also generates deformation-free palmprint images which can lead to higher matching accuracy as the ground truth information is better preserved as compared to those from contact-based imaging. Advancement of palmprint identification technologies for new domains requires research using larger palmprint databases that are acquired from more realistic population, under contactless, ambient, indoor and outdoor environments. This paper presents such a new contactless palmprint database acquired from 600 different subjects, which is the largest to-date and is also made available in public domain. Unlike contactless fingerprints, contactless palmprint images often illustrate pose deformations along the optical axis of camera, which also degrades the matching accuracy. This paper also introduces a new approach for matching contactless palmprint images using more accurate deformation alignment and matching. The experimental results are validated on three publicly available contactless palmprint databases. Comparative experimental results presented in this paper indicate consistently outperforming results over competing methods in the literature and validate the effectiveness of the investigated approach. These results also serve as baseline performance to advance much needed further research using most challenging and largest database introduced from this work.*

1. Introduction

Automated personal identification using physiological patterns and characteristics has been widely used in the civilian and law enforcement applications. Among a variety of popular biometrics identifiers, contactless hand-based biometrics identification offers higher user convenience due to ease in the presentation. Such hand-based user identification can be achieved with a range of hand-based biometric modalities, *e.g.*, fingerprint, finger knuckle, palmprint or palm vein. The choice of a specific biometric modality is largely influenced by the nature of business application and the level of security expected for the application. Identification of suspects by matching their leftover or the latent palmprint impressions with the contact-based impressions have been widely employed in the law enforcement departments around the world. Success of such applications has motivated the researchers to investigate palmprint identification using digital images and under contactless imaging setups.

Palmprint matching system is a typical pattern recognition system and relies on unique palm surface features that are to be robustly matched for achieving higher accuracy. The palmprint features historically employed for matching the latent and/or inked palmprint impressions can be divided into two categories, *i.e.*, the palmar flexion creases and palmar fiction ridges. The palmer fiction ridges from the raised portion of epidermis are same or similar to as those observed in typical fingerprint images and reveal variety of minutiae features. It is however difficult to observe palmar fiction ridges in palmprint images which have smaller resolution, *e.g*. less than 100 dpi images used in [3]-[15], [18]-[21]. In such images, palmar flexion creases and lines are the major source of information. Among three groups of flexion creases, the major flexion creases are widely considered to be the largest. The spatial arrangement of major flexion creases, *i.e*., distal transverse crease, proximal transverse crease, and radial transverse crease is identified in palmistry as the heart-line, head-line and life-line respectively. However, the uniqueness of such flexion creases is not sufficient to establish the identity and therefore these have been used for the alignment of palmprint images [1]. The digital palmprint images often reveal finger joint locations which are used as the reference points for the alignment of two palmprint images.

1.1 Related Work

Completely automated matching of palmprint images, acquired using the digital imaging setups, has received lot of attention from the researchers and a range of palmprint matchers have been introduced the literature. Such images typically reveal curved palmprint lines, creases and scars of varying thickness, instead of flexion ridges, and therefore a range of textured matching methods [3], [8], [10]-[13], [18]-[21] have been investigated to improve accuracy in matching these images. Such methods firstly generate well-aligned region of interest images by using finger joint locations as the reference points. This region of interest image is used to extract local palmprint features and matching is achieved using the best Hamming distance score generated from various translations or shifting of binarized templates. Such binalized representations are referred to as *PalmCode* and was generated from phase information using the Gabor filters. The dominant orientation of palm lines or creases at every pixel locations can ensure offer robustness in matching and such approach appears in [8]. The use of Gabor filters to recover palmprint features can be computationally complex as multiple real number multiplications are required at every pixels and therefore local Radon transform based approach to recover dominant palm line/crease orientation was introduced in [20] with outperforming results over the earlier methods. The success of this method in achieving superior matching accuracy is predominantly due to the local matching strategy, which was at the top of huge computational simplicity gained from the summation of local region pixels in computing features or the dominant orientations. Another successful approach for palmprint matching using binarized templates appears in [10] which incorporates derivative of Gaussian filters [21] to extract local features and the experimental results confirm superiority of this method in accurately matching palmprint images. Reference [35] for the first time provided theoretical analysis of such earlier works and develops *fast-CompCode*, *fast-RLOC* which have shown to offer significantly improved speed and the matching accuracy on multiple palmprint databases. A more simplified and more recent approach for the palmprint matching using the ordinal based spatial measurements appears in [9]. This approach models 3D palm surface as Lambertian surface and uses specialized masks for projective ordinal measurement that can reveal nature of the 3D palm surface from a single 2D palm image. A range of experimental results on most publicly available databases indicates that its best performing spatial domain methods for the palmprint matching.

A range of promising methods for matching the palmprint images using their frequency domain representations have also been developed in the literature. Reference [18] details such an approach that generates match score between two normalized palmprint images by computing normalized cross-correlation between the 2D FFT coefficients of the matched palmprint images.

In order to minimize the adverse influence of noise in matching such palmprints, authors only consider the FFT coefficients between predetermined threshold (band limiting) limits and such approach has shown its success in further improving the matching accuracy. Usage of discrete cosine transform coefficients extracted from *selected* local palmprint regions to accurately and more efficiently match contactless palmprint images is detailed in [3]. One of the most popular methods for matching two images with deformations and scale changes is to incorporate scale invariant feature transform [27]. Some of the promising efforts in the literature [13]-[14] therefore generate palmprint matching scores based on the number of such key points in two images. Earlier studies in the literature on contactless palmprint identification [32] have argued that the matching accuracy for less-constrained palmprint images can be enhanced by improving the registration accuracy among such images. The phase-based correspondence matching can offer better localization of corresponding points in two palmprint images under deformations and such approaches has shown [7] to offer outperforming results for the contactless palmprint matching.

The use of *contactless* palmprint images for personal identification has attracted attention of many researchers and now there are few contactless palmprint databases available in the public domain. The IITD touchless palmprint dataset [29] from 230 different subjects, GPDS contactless hands database [17] from 100 different subjects and KTU contactless palmprint database [4] from 145 different subjects. Reference [30] introduces contactless palmprint databases acquired from 301 different subjects and is believed to be the largest database in the public domain. More recently reference [37] introduces a contactless palmprint images database from 300 different subjects and provide encouraging results on the potential from this biometric. However, this dataset was acquired under indoor imaging environment, using a specially designed imaging setup, and therefore the imaging variations are small. Despite wide popularity of this database over last ten years, this database lacks images acquired under outdoor environment, with more realistic palms from the general public or by using a typical mobile camera. The development of contactless palmprint applications for real deployments requires database from larger subjects, acquired under outdoor and indoor imaging environment but without any special devices or illuminations and should include images from palms under presented under real deployment scenarios that can have dirt, write-ups or cosmetics.

1.2 This Work

A review of earlier work for the contactless palmprint recognition indicates great potential from this biometric for a range of e-security applications. Contactless palmprint recognition based on 2D images generally requires least expensive and more convenient image acquisition process which can be incorporated in a wide range of consumer devices and applications. Despite consistent improvement in the accuracy of palmprint matching algorithms during the last decade, further efforts are required to develop more accurate matching algorithms that can realize full potential from this biometric, particularly for matching palmprint images acquired from large number of subjects under real imaging environments. The contributions from this paper can now be summarized as in the following.

There are several publicly available palmprint databases in the literature for the researchers and much of the research advancements in this area can be attributed to the availability of these databases. However, the applications of palmprint identification technologies in new domains requires more realistic, contactless and larger databases that are acquired in outdoor environment. This paper presents a new contactless palmprint database towards such goal. This publicly available database has been acquired from 600 different subjects, which is the *largest to-date*, under contactless and more realistic environments. Unlike other public palmprint image database available for the researchers, this database provides images from non-office subjects (*e.g*. hands from manual laborers, injury, cosmetics, *etc*.). Most importantly, this database also provides palm images acquired from very long interval (15+ years) that will enable further study on the temporal stability of palmprint biometrics for civilian and forensic applications. Additionally, this paper also details the development of more promising and accurate approach for the contactless palmprint matching. This new approach is developed by addressing limitations of earlier palmprint matching methods in computing local pixel-level transformations for frequent deformations observed in palmprint images and by incorporating spatial-domain but noise tolerant local matching scheme for corresponding regions in the two palmprint images. This entire approach is systematically detailed in section 2 and has been evaluated on three different publicly available contactless palmprint images databases. Experimental results presented in section 3 indicate consistently outperforming results over other competing methods in the literature for matching contactless palmprint images and therefore validate the usefulness of the contactless palmprint matching approach introduced in section 2. The key objective of presenting experimental results from most competing methods, including best performing one from this paper, is to provide a baseline for largest contactless palmprint database to enable much needed further work in this area.

The rest of this paper is organized as follows. Section 2 systematically presents a more effective approach for the contactless palmprint image alignment and matching. The details on the new contactless palmprint database, along with other databases employed in the experiments, appears in section 3. Comparative experimental results from the most competing methods, using respective databases, are also are presented in section 3. Section 4 provides a critical discussion on the database and the method introduced in section 2. This section also provides palmprint image samples from the same subjects/hands acquired after an interval of 15+ years. Finally, the key conclusions from this work are summarized in section 4.

2. Contactless Palmprint Image Alignment and Matching

Contactless palmprint images are expected to present higher intra-class variations, as compared with the contact-based palmprint images, largely due to the nature of contactless imaging. Therefore, one of the key challenge for improving the matching accuracy from contactless palmprint images lies in the accurate alignment of region of interest images. Undesirable small rotations of palm (yaw, pitch, roll) with respect to the optical axis of the camera, during the contactless imaging, is the key reason for the observed deformations in the region of interest images which are generated after the segmentation process. Such segmentation [25] of region of interest (ROI) images should ensure that same palm region is recovered in such a manner that the pose of such regions is always aligned in the same direction as much possible. Therefore, key focus of this work was to ensure best possible alignment of the local regions, *i.e.*, image blocks, as this can also address frequently observed deformations in the contactless palmprint images. Given two contactless palmprint ROI images, we wish to know if they belong to the same hand or not. The algorithm to match such ROI images can be broadly divided into three steps, **(i)** identifying the grid map between two image (explained in section 2.1), **(ii)** extracting local blocks around each of the selected grid points (explained in section 2.2), and **(iii)** comparing the corresponding blocks from the two images to generate the matching score (explained in section 2.3).

2.1 Localizing and Mapping Grid Points

Let the image f be the reference palmprint ROI image and the image g be the presented or query palmprint ROI image to be matched. These images are expected to be of the same size as they

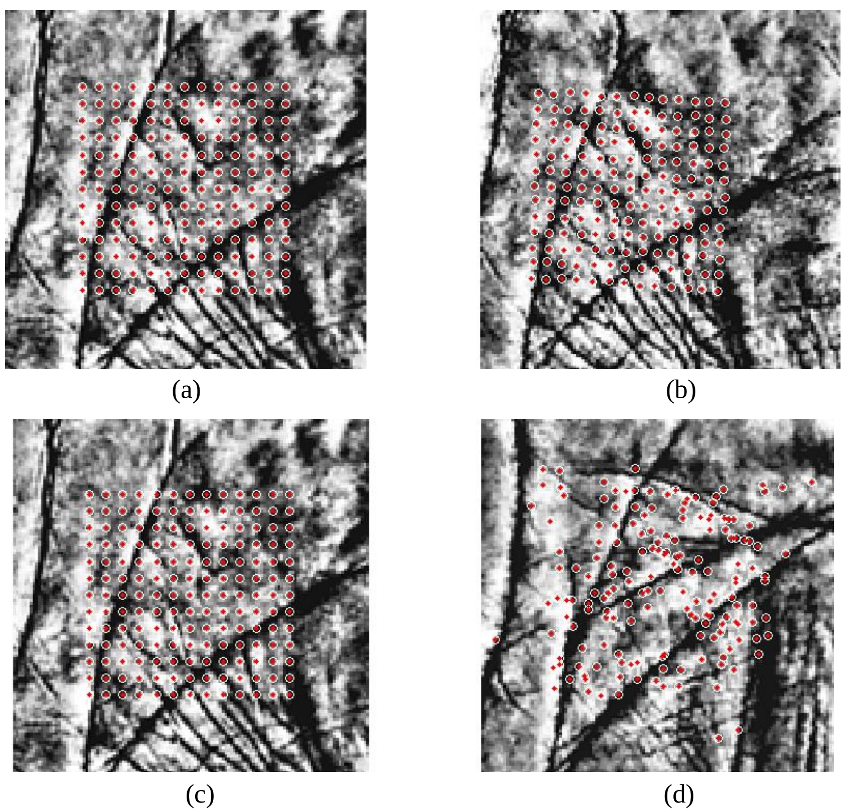

Figure 1: Sample palmprint images with respective grid-maps: the pair (a)-(b) illustrates the grid-map for same subject (genuine match) while paid (c)-(d) illustrates the grid-map for different subject (imposter match).

represent region of interest extracted after the image normalization process. The reference image is firstly marked with $n \times n$ grid using equally spaced points. For example when the normalized ROI images are of 128×128 pixels (as for many experiments in this paper), if we use $n = 13$ with a spacing of 6 pixels between the neighboring points, we can obtain the grid points as shown in figure 1 (a). In such reference image, the first point is positioned at $(28, 28)$ and the last point is at $(100,100)$.

Assuming finite number of grid points in the reference image *f*, each of these grid points $\boldsymbol{p}^0$ on the reference image f are mapped to point $\boldsymbol{q}^0$ on the query image g. This strategy for locating corresponding grid points between any two images is detailed in [26] and is incorporated for our problem by using a three-layer image pyramid for the mapping. The following is the algorithm for obtaining $\boldsymbol{q}^0$ given grid point $\boldsymbol{p}^0$.

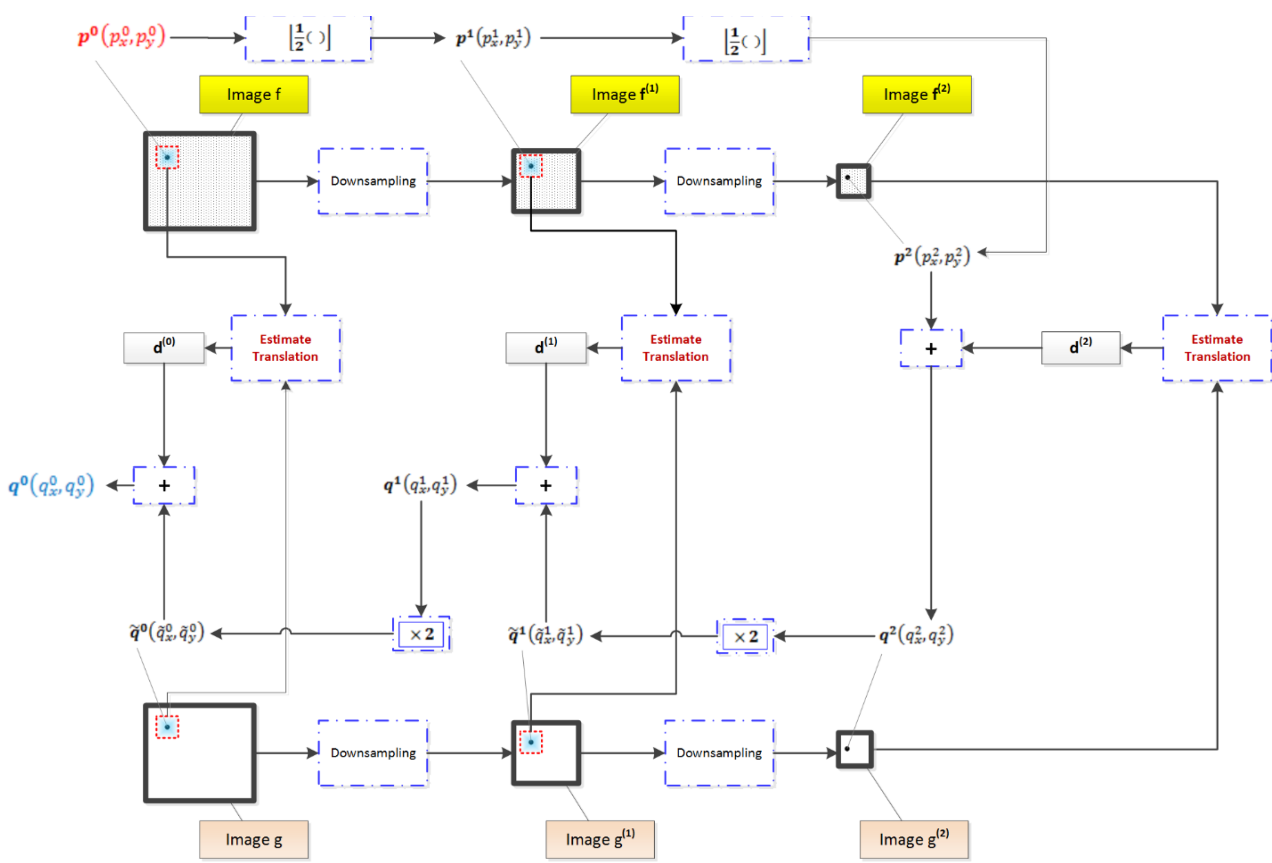

Figure 2: Block diagram representing the mapping process for point p^o in image ***f*** to the point q^o in image ***g***.

(a) Given the images in layer $l-1$, the l^{th} layer images are obtained as follows:

$$f^l(i,j) = \frac{1}{4}\sum_{k_1=0}^{1}\sum_{k_2=0}^{1} f^{l-1}(2i+k_1, 2j+k_2) \quad (1)$$

$$g^l(i,j) = \frac{1}{4}\sum_{k_1=0}^{1}\sum_{k_2=0}^{1} g^{l-1}(2i+k_1, 2j+k_2) \quad (2)$$

where from f^0 $(= f)$ and g^0 $(= g)$, we can recover f^1, f^2 and g^1, g^2.

(b) The grid points $\boldsymbol{p}^1$ in f^1 and $\boldsymbol{p}^2$ in f^2 corresponding to the given point $\boldsymbol{p}^0$ in f^0 are obtained as follows:

$$\boldsymbol{p}^1 = \left\lfloor \frac{1}{2}\boldsymbol{p}^0 \right\rfloor \quad (3)$$

$$\boldsymbol{p}^2 = \left\lfloor \frac{1}{2}\boldsymbol{p}^1 \right\rfloor \quad (4)$$

where $\lfloor x \rfloor$ represents the floor operation *i.e.* rounding the number x to the nearest integer towards negative infinity.

(c) Next step is to estimate the extent of displacement between the images f^2 and g^2. This is achieved by computing the displacement vector be $\boldsymbol{d}^2$. Here we make assumption that the layer $l = 2$ is coarse enough such that the estimated $\boldsymbol{d}^2$ is accurate, *i.e.*, $\boldsymbol{q}^2 = \boldsymbol{p}^2 + \boldsymbol{d}^2$.

(d) For $l = 1$, let the approximate value of $\boldsymbol{q}^l$ be represented by $\widetilde{\boldsymbol{q}}^l$ and this can be computed using $\widetilde{\boldsymbol{q}}^l = 2\boldsymbol{q}^{l+1}$ as shown in figure 2. The next step is to extract local blocks of size $W \times W$ pixels around the points $\boldsymbol{p}^l$ and $\widetilde{\boldsymbol{q}}^l$ in the images f^l and g^l.These blocks can be represented as f_b^l and g_b^l. The extent of the block size is empirically determined and fixed as $W = 39$ for all the experiments in this paper.

(e) Again estimate the displacement between the blocks f_b^l and g_b^l. Let this displacement be represented as $\boldsymbol{d}^l$. The exact location of $\boldsymbol{q}^l$ can be estimated as follows:

$$\boldsymbol{q}^l = \widetilde{\boldsymbol{q}}^l + \boldsymbol{d}^l \quad (5)$$

(f) Repeat above steps in (d) and (e) for $l = 0$, to compute $\boldsymbol{q}^0$ (figure 2).

Above steps are repeated for the every grid point and thus the grid-map for the images f and g is obtained. The images in figure 1 illustrates examples of grid-maps corresponding to a genuine match and an imposter match.

2.2 Estimating Local Palmprint Translations

The translation between two palmprint sub-images can be computed from the Fourier shift property [36] which states that the translational changes between two images are transformed in the spectral domain as their linear phase differences. In order to accurately estimate such translations for the steps shown in figure 2, the method incorporated in [7] was further modified. Given two palmprint ROI images $f(n_1, n_2)$ and $g(n_1, n_2)$, the translation error between them is estimated as follows:

(a) Let the dimensions of these images be $N_1 \times N_2$ while $M_1 = \frac{N_1 - 1}{2}$ and $M_2 = \frac{N_2 - 1}{2}$. The index ranges of pixels are assumed to be $n_1 = -M_1, \dots, M_1$ and $n_2 = -M_2, \dots, M_2$ for the mathematical simplicity.

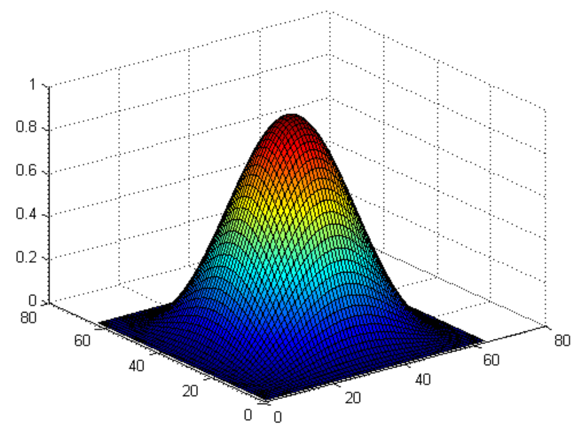

Figure 3: Hanning window function employed to reduce edge artifacts from local palmprint regions.

(b) A popular method for computing translation between two images is to use phase correlation that relies on the translation property of 2D FFT, *i.e.* shift theorem [22]. This 2D FFT operation required to estimate such translation between two images assumes that 2D image data is periodic. However for our problem the 2D Discrete Fourier Transforms (DFT) operation is only applied to a small region of interest image which often results in edge artifacts at the border. The adverse effect of such discontinuities is reduced by employing a 2D window function. This function $h(n_1, n_2)$ is applied (Figure 3-4) to both of the palmprint images f and g and can be defined as in the following:

$$h(n_1, n_2) = \frac{1+\cos\left(\frac{\pi n_1}{M_1}\right)}{2} \times \frac{1+\cos\left(\frac{\pi n_2}{M_2}\right)}{2} \quad (6)$$

where $n_1 = -M_1, \dots, M_1$ and $n_2 = -M_2, \dots, M_2$. The resulting images following this operation is represented as f_h and g_h.

(c) The images f_h and g_h from above operations are used to compute 2D FFT. These can be represented as $F(k_1, k_2)$ and $G(k_1, k_2)$, and respectively obtained as follows:

$$F(k_1, k_2) = \sum_{n_1=-M_1}^{M_1} \sum_{n_2=-M_2}^{M_2} f_h(n_1, n_2) W_{N_1}^{k_1 n_1} W_{N_2}^{k_2 n_2} \quad (7)$$

$$G(k_1, k_2) = \sum_{n_1=-M_1}^{M_1} \sum_{n_2=-M_2}^{M_2} g_h(n_1, n_2) W_{N_1}^{k_1 n_1} W_{N_2}^{k_2 n_2} \quad (8)$$

where $k_1 = -M_1, \dots, M_1$, $k_2 = -M_2, \dots, M_2$, $W_{N_1} = e^{-j\frac{2\pi}{N_1}}$, $W_{N_2} = e^{-j\frac{2\pi}{N_2}}$.

(d) Translation between two palmprint images (from the same subject) can be related to their phase differences in their frequency domain representations. Therefore the normalized cross-phase spectrum $\hat{R}(k_1, k_2)$ between two ROI images is computed next and is generated as in the following:

$$\hat{R}(k_1, k_2) = \frac{F(k_1,k_2)\,\overline{G(k_1,k_2)}}{\left|F(k_1,k_2)\,\overline{G(k_1,k_2)}\right|} \quad (9)$$

where $\overline{G(k_1, k_2)}$ is the complex conjugate of $G(k_1, k_2)$.

(e) Low-spatial frequency components in palmprint images, *e.g.* major palm lines, are expected to be more stable as compared with the high spatial frequency components representing minor creases and noise. Therefore the accuracy in the estimation of translation can be improved by excluding high spatial frequency components in $\hat{R}(k_1, k_2)$ by using a low-pass filter $L(k_1, k_2)$ which can be defined as follows:

$$L(k_1, k_2) = \begin{cases} 1, & |k_1| \le C_1, |k_2| \le C_2 \\ 0, & \text{otherwise} \end{cases} \quad (10)$$

where C_1, C_2 are integers that represent cut-off frequency with respective constraints $0 \leq C_1 \leq M_1$ and $0 \leq C_2 \leq M_2$. The experiments detailed in this paper used $C_1 = \left\lceil \frac{M_1}{2} \right\rceil$ and $C = \left\lceil \frac{M_2}{2} \right\rceil$.

(f) Let $\widehat{R_L}(k_1, k_2) = \hat{R}(k_1, k_2) \times L(k_1, k_2)$ represent output obtained from low-pass filtering operation using (10). The band-limited normalized cross-phase spectrum $\widehat{R_L}(k_1, k_2)$ is now zero-padded to obtain $\hat{R}_L^u(k_1, k_2)$. The size of $\widehat{R_L}(k_1, k_2)$ is $C_1 \times C_2$ and after zero-padding, the size of $\hat{R}_L^u(k_1, k_2)$ is enhanced to $uN_1 \times uN_2$, where u is the up-sampling factor and is empirically fixed to $u = 4$ for all the experiments in this paper.

(g) The inverse discrete Fourier transform of $\hat{R}_L^u(k_1, k_2)$ represents phase differences in the frequency domain representations. This phase only correlation measure $\hat{r}(n_1, n_2)$ is computed as follows:

$$\hat{r}(n_1, n_2) = \frac{1}{N_1 N_2} \sum_{k_1=-M_1}^{M_1} \sum_{k_2=-M_2}^{M_2} \hat{R}_L^u(k_1, k_2) W_{N_1}^{-k_1 n_1} W_{N_2}^{-k_2 n_2} \tag{11}$$

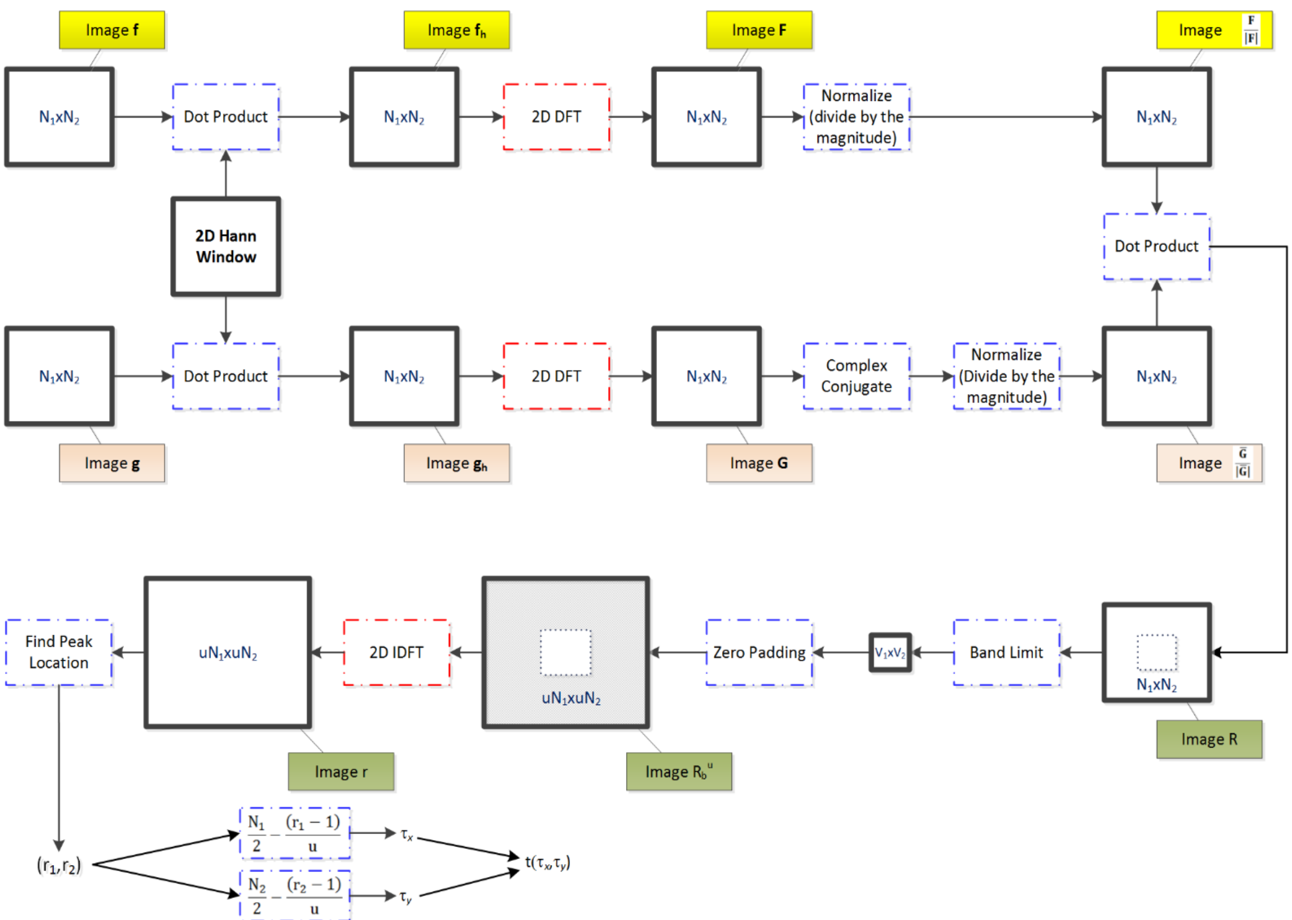

Figure 4: Block diagram for estimaing translation ***t*** between the two palmprint images ***f*** and ***g***.

(h) The position of peak (maximum value) in (11) is located to estimate the extent of translational error between two normalized (ROI) images. Let this location be represented as (r_1, r_2), where r_1 is the *row* number for the maximum value in the matrix $\hat{r}$ and r_2 is the corresponding *column* number. Then the translation error (τ_x, τ_y) between the images $f(n_1, n_2)$ and $g(n_1, n_2)$ can be computed as follows:

$$\tau_x = \frac{N_1}{2} - \frac{(r_1 - 1)}{u}, \quad \tau_y = \frac{N_2}{2} - \frac{(r_2 - 1)}{u} \tag{12}$$

The zero-padding operation in step (e) to suppress high frequency components can be avoided if a function fitting approach is employed to locate the translation error. The cross-power spectrum between two such spatially translated images has a particular structure, which can be exploited for this purpose. Foroosh *et al*. [33] have shown that the phase correlation between two images leads to downsampled 2-D Dirichlet kernel which can be very closely approximated by a 2-D sinc function. They have also provided an analytical expression for sub-pixel shift estimation, under low-pass filtering of cross-phase spectrum, which can be used to simplify $\hat{r}(n_1, n_2)$ between two palmprint images as follows:

$$\hat{r}(n_1, n_2) \cong \frac{1}{S\,N_1 N_2} \frac{\sin\left\{\frac{D_1}{N_1}\pi(n_1 + \tau_x)\right\}}{\sin\left\{\frac{\pi}{N_1}(n_1 + \tau_x)\right\}} \frac{\sin\left\{\frac{D_2}{N_2}\pi\left(n_2 + \tau_y\right)\right\}}{\sin\left\{\frac{\pi}{N_2}\left(n_2 + \tau_y\right)\right\}} \tag{13}$$

where S is some positive constant $S \geq 1$, $D_1 = 2C_1 + 1$ and $D_2 = 2C_2 + 1$. The data array $\hat{r}(n_1, n_2)$ obtained from the two images $f(n_1, n_2)$ and $g(n_1, n_2)$ is fitted to the above function and the required parameters τ_1 and τ_2 are estimated. For this purpose, a local region (say 5×5 data points) around the maximum peak in the phase only correlation array is adequate for the fitting and employed for the experiments in this paper.

2.3 Generating Match Scores

Once the corresponding grid maps for a pair of palmprint images are located, a block of size $W_b \times W_b$ pixels is automatically extracted around each of the grid point in both the ROI images. Matching such image blocks using spectral domain features can degrade the performance as the effect of noise, aliasing and border effects are mostly present in the spectrum (2D DFT) of these images. The match score for each of the $n \times n$ corresponding image block pairs, say f_b and g_b, is therefore computed in spatial domain. This match score between such corresponding blocks is computed using their grey level similarity. A spatial filter is employed to perform convolution with every block f_b and g_b. This spatial filter $w(x, y)$ [24] can be defined as follows:

$$w(x,y) = \begin{cases} 1 & if\ abs(x) < abs(y) \\ -1 & if\ abs(x) > abs(y) \\ 0 & if\ abs(x) = abs(y) \end{cases} \tag{14}$$

where x, y represents spatial locations in the filter with $x, y \in \left[-W_f, W_f\right]$ and $abs(\cdot)$ is the absolute operation. The binarized features for the image block f_b (or g_b) is computed as follows:

$$F_b(x,y) = \begin{cases} 1 & if\ f_b(x,y) * w(x,y) > 0 \\ 0 & otherwise \end{cases} \tag{15}$$

where $*$ represents pixel-wise convolution operation. In order to minimize the influence from the undesirable noise in the binarized templates for each of the blocks, these templates are subjected to morphological operations similar to as in [9]. Therefore morphological opening and closing operations are performed on each of the binarized feature maps from (15) to generate two more feature maps, *i.e.* F_b^o, F_b^c and G_b^o and G_b^c respectively for image block f_b and g_b. The combination of Hamming distances between these templates is used to compute match scores between image blocks. The consolidated match score $s_{f,g}$ is computed using the average of ($n \times n$) match scores between the corresponding image blocks in two palmprint ROI image f and g as follows:

$$\begin{aligned} s_{f,g} = \frac{1}{n \times n} \Bigg\{ & \frac{c_1}{(W_b - q1)(W_b - p1)} \sum_{y=1}^{W_b - p1} \sum_{x=1}^{W_b - q1} XOR(F_b, G_b) \\ & + \frac{c_2}{(W_b - q2)(W_b - p2)} \sum_{y=1}^{W_b - p1} \sum_{x=1}^{W_b - q1} XOR(F_b^o, G_b^o) \\ & + \frac{c_3}{(W_b - q_3)(W_b - p_3)} \sum_{y=1}^{W_b - p1} \sum_{x=1}^{W_b - q1} XOR(F_b^c, G_b^c) + \Bigg\} \end{aligned} \tag{16}$$

where $XOR(H, E)$ represents the Boolean XOR operator that computes Hamming distance between two binarized template, *e.g*. between H and E, $n \times n$ is the number of grid points, $W_b \times W_b$ is the spatial size of block, while c_1, c_2, c_3 represents respective weightage for the denoised templates. In order to accommodate local deformations between the corresponding grid points, respective binarized templates are translated in the horizontal (q_1) and vertical direction (p_1) to perform multiple matches. These translations are performed for four directions (left, right, up, down) in the steps of two pixels. The best or the smallest of Hamming distance among such translations, *e.g*., achieved at (p_1, q_1), and is used as the final similarity score from the respective template. All the experiments in this paper employed $n = 13$, W_f=11, c_1=3, c_2= $c_3 = 1$, W_b=39 and these parameters were empirically fixed. The consolidated match score $s_{f,g}$ between two palmprint ROI images is used assign the matched pairs to one of the two classes, *i.e.*, genuine or impostor.

3. Experiments and Results

Several experiments were performed using the publicly available contactless palmprint databases to ascertain the effectiveness of method detailed in previous section. In this section, the publicly available contactless palmprint databases employed for the performance evaluation are firstly

Figure 5: Image samples from publicly available contactless palmprint databases used in experiments; (a) hand image and respective segmented palmprint image from IITD palmprint database, (b) hand image samples from CASIA palmprint database along with respective segmented palmprint images.

described. We then introduce a new contactless palmprint database which is now made publicly available [23]. The experimental results are provided along with the details for the respective database.

3.1 IITD Touchless Palmprint Database

The IITD touchless palmprint database [30] provides contactless palmprint images from right and left hands of 230 subjects. This database also provides 150 × 150 pixels segmented palmprint images from each of the hands. There are five samples for each of the right and left hand palmprint images in the database. Figure 5 illustrates samples of palmprint images, along with their automatically segmented palmprint images, from this database. Similar to as in [9], all the 1150 palmprint images from the right hand were used in the experiments for the performance evaluation. Therefore a total of 2300 genuine and 1,316,750 impostor match scores were generated for respective experiments using the segmented palmprint images provided from this database. The receiver operating characteristics (ROC) using IITD touchless palmprint database is shown in figure 6. This figure also illustrates comparative performance using other competing methods reported in earlier work.

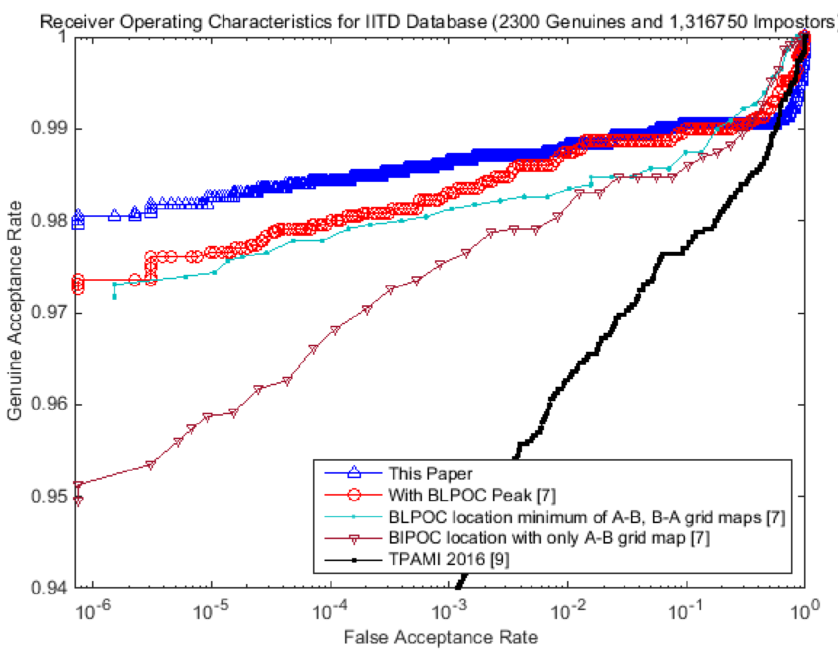

Figure 6: Experimental results from Contactless IITD palmprint database using ROC.

The palmprint matching method detailed in reference [9] has shown to achieve best performing results over the other methods (like CompCode [8], Ordinal [10], RLOC [20]) on publicly available palmprint databases and therefore this method was appropriately used as the baseline for the performance evaluation. Similarly, the method introduced in [7], using correspondence point matching is the most promising frequency domain method for matching contactless palmprint images (*e.g*. for CASIA palmprint database) and has also shown outperforming results over many other methods in the literature. Therefore, this method was also judiciously selected as another baseline to ascertain the performance. It may be noted that matching two palmprint images using [7] with the method of correspondence points locations can generate different scores when image A is matched with image B as compared to the case when image B is matched with image A (for example). Therefore both of these combinations, along with the best of match scores, generated from matching A with B and B with A, were also investigated for any possible performance improvement. It can be observed from the experimental results in figure 6 that performance from such approach is poor than from BLPOC peak score. The performance from BLPOC location based approach is poor than those from BLPOC location peak score based approach. Therefore the BLPOC peak score approach was judiciously selected as a baseline for further comparative evaluation in this paper. Table 1 presents the equal error rate (EER) using different methods used for the initial performance evaluation. These

Table 1: Comparative EER for Contactless Palmprint Matching using IITD Database.

Method	EER
This Paper	1.17
BLPOC Peak score [7]	1.22
BLPOC Location based [7]	1.69
BLPOC Location based with min (A-B and B-A)	1.55
DoN-TPAMI [9]	3.02

experimental results in Figure 6 and Table 1 indicates that the method detailed in section 2 achieves superior performance.

3,2 CASIA Palmprint Database

The CASIA palmprint database [31] is another contactless palmprint database with 5239 palmprint images from 301 individuals which is the largest public dataset used in earlier publications. It is the largest publicly available database in terms of the number of individuals. As also explained in [9], the individual "101" in this database is the same as the individual "19" and therefore these two classes were merged into one class. The 11th image from the left hand of individual "270" is also misplaced to the right hand. The 3rd image from left hand of individual "76" is a distorted sample with very poor image quality. Similar to as in [9], these two samples can also be automatically detected by the palmprint segmentation program. These two images were eliminated in our experiment. Therefore the experiments using this database employed 5237 images from 600 different palms. All the images were automatically normalized and segmented using simple image processing operations. These segmented or resulting ROI images were scaled to 128 × 128 pixels and

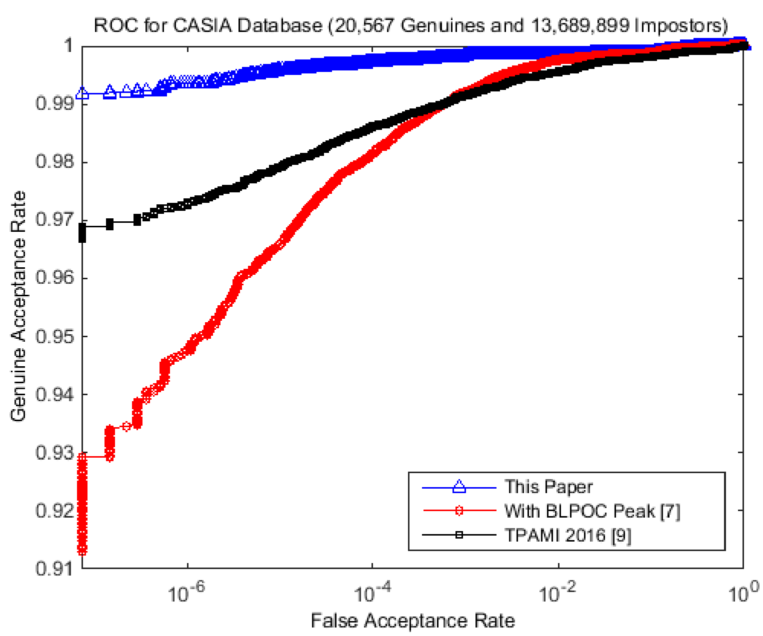

Figure 7: Experimental results from CASIA palmprint database using ROC.

used for generating the match scores. The total number of genuine match scores were 20,567 and the total number of impostor match scores were 13,689,899. The EER for the method in [9], using the best performing method in [7] and the method detailed in section 2 is 0.529%, 0.402% and 0.126% respectively. The respective ROC for different experiments on this dataset is shown in figure 7. These experimental results also indicate outperforming results using the method detailed in section 2.

3.3 PolyU-IITD Contactless Palmprint Database Version 3.0

This new palmprint database has been acquired over several years from 600 different subjects which is largest to-date and each subject in this database provided his/her left and right hand images. A handheld digital camera was used to acquire the images while volunteers presented their hands for the imaging with different hand poses. The images in this database therefore also have high scale variations and are acquired from subjects as small as 5 years old to 72 years old. Almost 200 subject's images in this database are from the Chinese while the majority of subjects images in this database are from Indians. It may be noted that IITD database or CASIA database has all subject's images from the same ethnicity (almost all images in CASIA database are from Chinese ethnicity while all subjects in IITD database are Indians). The images were acquired using more than one two digital cameras and the minimum size of the acquired image in this database is 1280×960 pixels while the maximum size is 4352×3264 pixels. More details regarding the images (*e,g*, camera used) can be read from the header information available with respective images. All the images were acquired under indoor or the outdoor environment without any external or fixed illumination. The imaging under such ambient illumination are representative of images expected from a typical contactless palmprint identification application using mobile devices. One of the unique features of this database is that it includes large number of images acquired from non-office workers or images acquired from manual and countryside labourers, children in primary and secondary schools in rural

Figure 8: Sample images from hands of *different* subjects in the new contactless palmprint database: first row depicts image samples from subjects with palm injury or with special capabilities, second row depicts image samples from manual or agricultural workers in country side, third row depicts samples from subjects with handwritten text (as an aid for memory) and the last row depicts samples from subjects with cosmetics (a popular cultural practice among the rural and some urban population).

areas, and images from hands with special abilities (*e.g.* six fingers) or with the injuries. In summary, the new database introduced in this paper not only has largest subject population as compared to any other existing palmprint database, but it also includes palmprint images from subjects under different cultural background and occupations which are acquired under contactless and ambient illumination conditions. Therefore this database is expected to present a notable addition for the advancement of palmprint research for contactless applications. Figure 8 illustrates typical palmprint image samples from this database.

All the palmprint images in this database were automatically segmented and the segmentation is achieved using the method similar to as detailed in [25]. The contactless

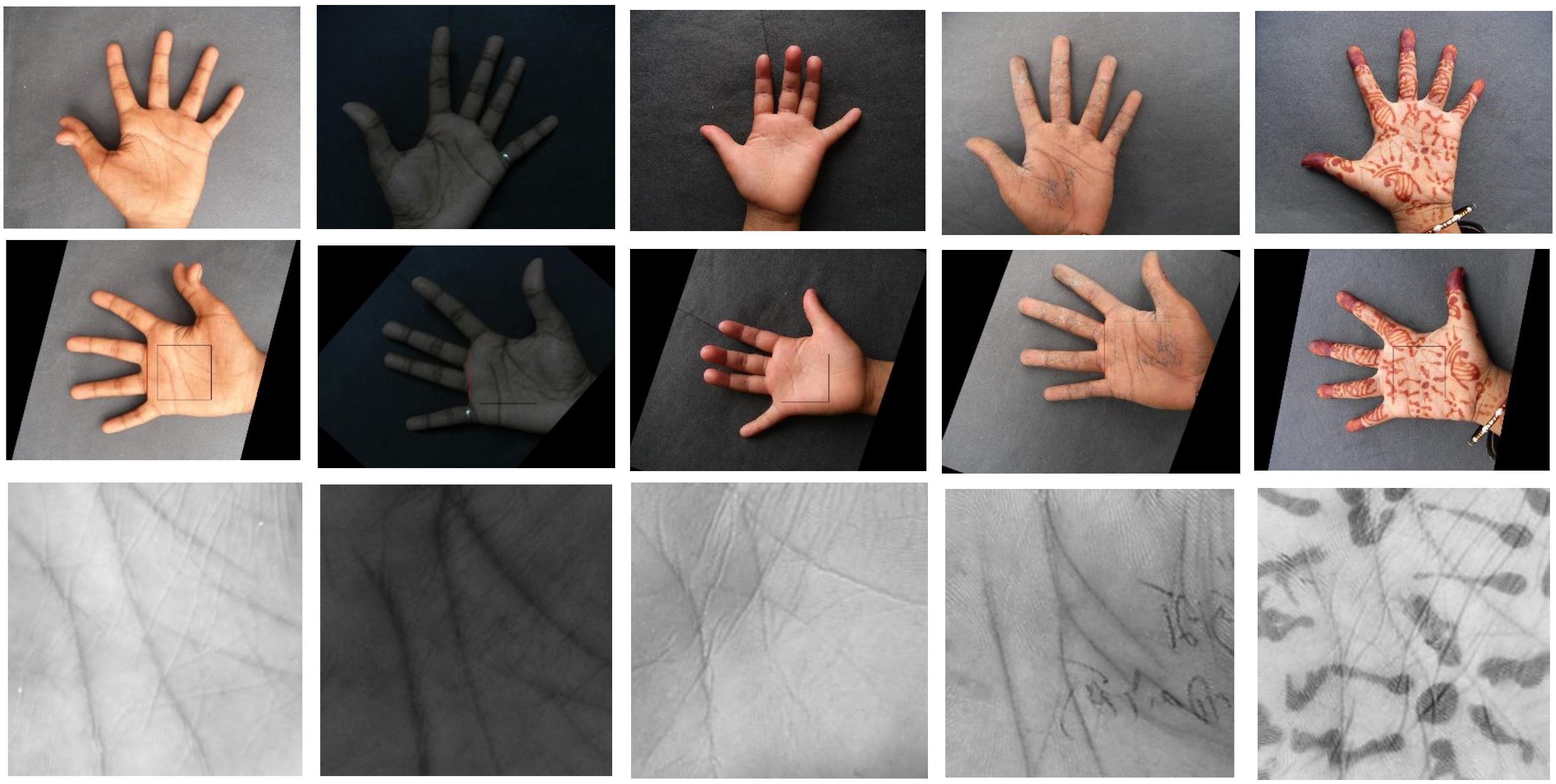

Figure 9: Image samples from the new contactless palmprint database along with their respective segmented and normalized region of interest images used in the experiments.

palmprint images are expected to have significantly higher scale and pose variations. Therefore, respective palmprint segmentation approach should ensure that intra-class variations in the segmented ROI images are minimized. The palmprint region of interest is extracted relative to the scale of acquired image and the segmented image is then scaled to a fixed size image for the matching. This is achieved by firstly localizing the two key points, *i.e.*, the joint between the index and middle finger, and the joint between the ring and little finger. The segmented palmprint region is therefore *relative* to the distance between these two key points and oriented along the normal joining these points. Figure 9 presents some sample images from this database and its corresponding segmented images. This figure also illustrates intermediate step images with *exact* region of interest (the square in blue color on the images in middle row) which is segmented after the alignment of input image. This publicly available palmprint database also provides the segmented images, both in greyscale and color, which is expected advance much needed further research work in this area.

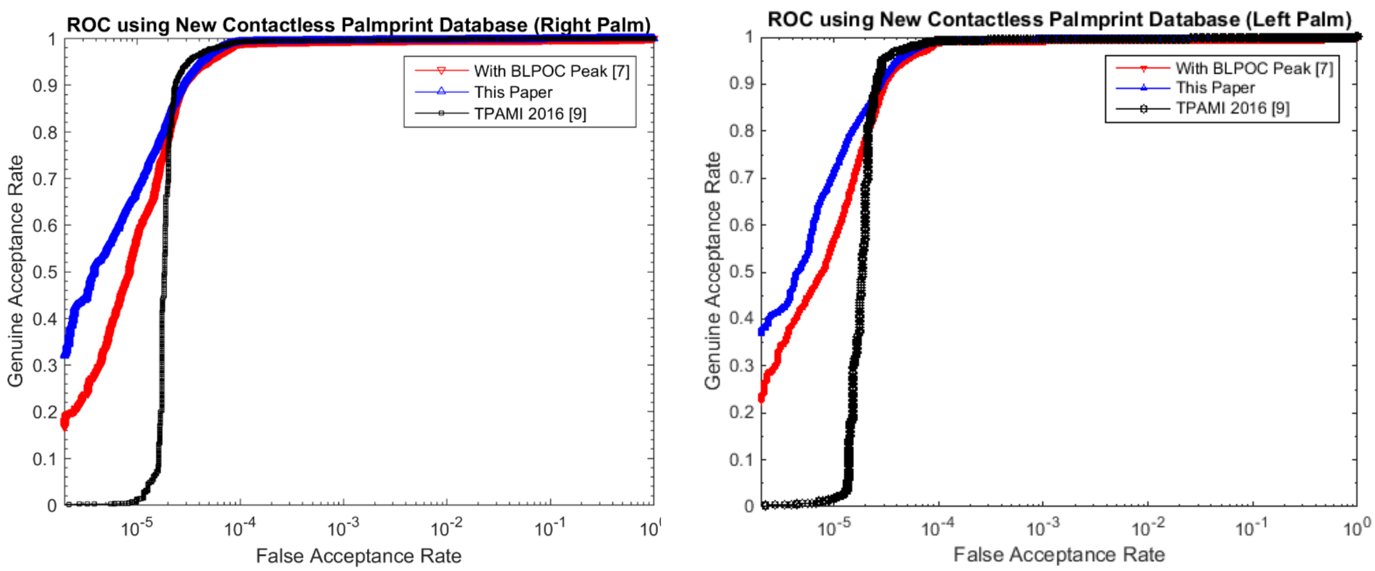

(a) (b)

Figure 10: Experimental results using (a) right hand images and (b) left hand images in the new palmprint database from 600 subjects.

The experiments using this new database were performed using all the ten images from each of the left and right hand palmprint images. Therefore, each of the experiments for the palmprint matching generated 6000 genuine scores and 3,594,000 impostor scores. The ROC's corresponding to the respective experiments using right hand palmprint ROI images are illustrated in Figure 10(a). The EER from the method in [9], using the best performing method in [7] and the method detailed in section 2 is 0.331%, 0.46% and 0.45% respectively. Similarly, the ROC's corresponding to the experiments using the left hand palmprint images from all the 600 subjects are illustrated in Figure 10(b). The EER from the method in [9], using the best performing method in [7] and the method detailed in section 2 is 0.33%, 0.50% and 0.52% respectively. The experimental results illustrated in figure 10(a)-(b) consistently indicate superior performance from the proposed approach using new contactless palmprint database.

4. Discussion

One critics of the newly introduced database in previous section is that it is largely a single session database and two session database is expected to provide more reliable estimate on performance under deployment scenarios. However, it should be noted that in any two-session public palmprint

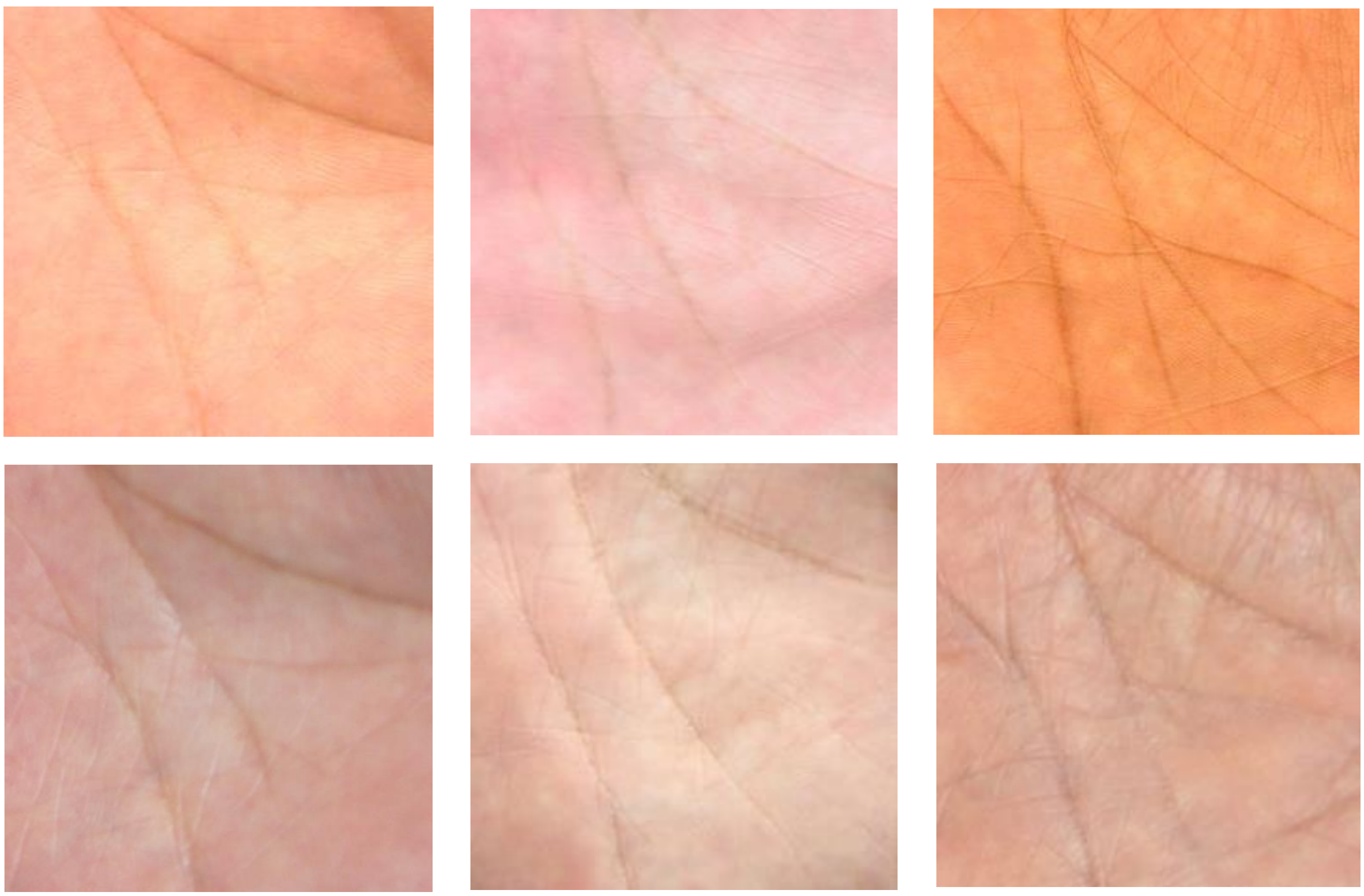

Figure 11: Sample left hand palmprint images in first row and *corresponding* palmprint image in the second row acquired after 15+ years.

databases, *e.g*. [28], the separation of two sessions is quite small (6-8 weeks) which is not adequate to capture temporal variations as the palmprint patterns are known to be quite stable among adults. The temporal variations in the palmprints could be captured when the interval between sessions are quite large (at least one year). The intra-class variations introduced during the contactless palmprint imaging are much higher than contact based imaging, or those due to the short-term temporal variations, and the objective of the new database is to evaluate inter-class identification capabilities from the palmprint modality from large number of subjects instead of presenting claims on the stability of palmprint patterns. However, probably for the first time in the palmprint literature, figure 11-12 presents set of palmprint images acquired after 15 years of interval from the subject. Although these images are presented in color, the color changes can also be due to the changes in camera and the ambient illumination during the imaging. A careful look at the corresponding lines and creases, between the images in the first row and the corresponding image in the second row, indicates that stability of these features even after such long interval. There are

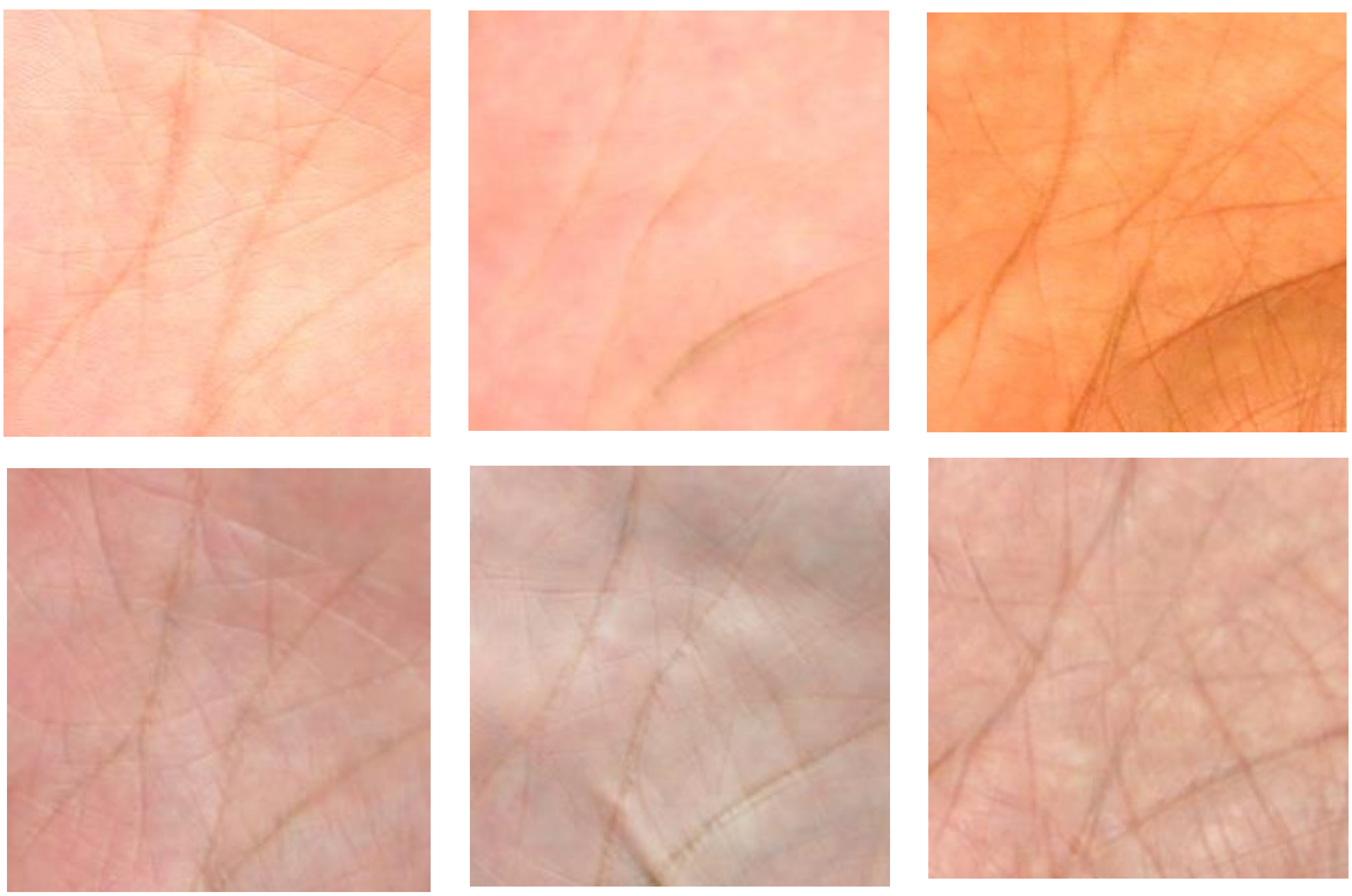

Figure 12: Sample right hand palmprint images in first row and *corresponding* palmprint image in the second row acquired after 15+ years.

many such long interval palmprint image sample pairs included in this new database to enable further study on the temporal variations in respective images acquired over the large interval.

The comparative experimental results from the two-session contactless palmprint images are illustrated in figure 13 using the ROC. These experiments were performed using twosession images from the database of 35 different subjects' right hand palm images. All of these two-session palmprint images, along with respective segmented images used in the experiments, are publicly made available from this dataset. The first session for each subject had five images in these experiments and second session also utilized five images. Therefore 175 (5×35) genuine and 5950 ($5 \times 35 \times 34$) impostor scores were generated for each of the experiments. Figure 14 presents match scores from two-session sample images acquired after 15+ year's interval, along with the decision threshold corresponding to EER. The ROC from three comparative methods in figure 13 indicate that the method detailed in section 2 can achieve outperforming results. The equal error rate from the method in [9], using the best performing method in [7] and the method introduced in this paper is 0.2629, 0.2514 and 0.2051 respectively. Comparing the experimental results in figure 13 and those in figure 10, it can be observed that the method introduced in section 2 of this paper consistently offers outperforming results over the other baseline method. Despite such promising results, the performance achieved from two session experiments indicates high error rate and such

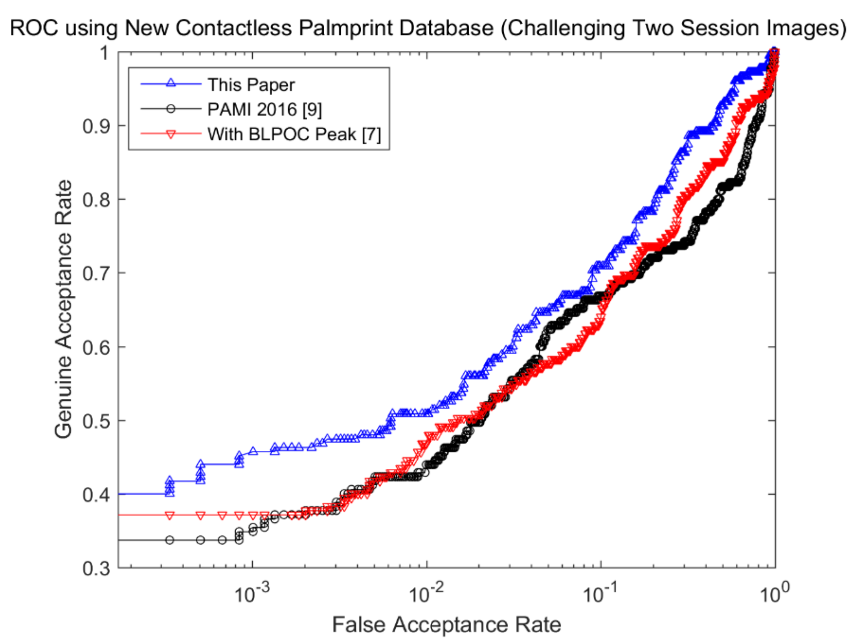

Figure 13: Comparative experimental results from two-session challenging images dataset.

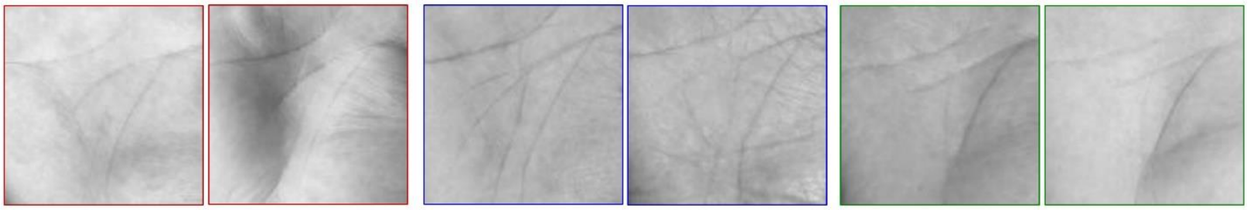

(a) Match score: 1.1889 (b) Match score: 0.872 (c) Match score: 0.739

Figure 14: Match scores from long interval sample images. First images in above three sets were acquired in year 2001-2002 while the second session images on the right were acquired in 2017. All three sets of images generate match scores smaller than decision threshold (1.233) and therefore can be considered as matched using the best performing method from this paper.

degradation in matching accuracy can be attributed to the challenging images acquired during the second session imaging resulting from the long-interval imaging, cosmetics or the handwritten text. Availability of such challenging two-session dataset from this work in public domain can enable much needed further work to further improve the performance for real-world contactless palmprint identification applications.

Sub-pixel and pixel-level correspondence points should be locally matched, instead of globally, to maximally benefit from local matches that can be undermined in any global matching strategy. Therefore this paper utilized such matching strategy in section 2.3 and also incorporated better sub-pixel level displacement estimation between the images in section 2.2 by suppressing high-frequency contents from the cross-phase spectrum and by incorporating closed-form analytical solution [37] to estimate positions of spectral peaks. This matching strategy can also account for noise and has resulted in a new approach, which is specifically suitable for contactless palmprint images that often have local deformations and aided by noise. The experimental results presented in section 3 on three different publicly available contactless palmprint databases consistently indicate outperforming results. Among these, the performance improvement for the largest database from 600 different subjects is significant, as can be observed from the ROCs in figure 10 (with 36.7% and 34% improvement in EER), and can be considered as more reliable indicator for comparative performance. It should also be noted that all the parameters for matching palmprint images were *same* for different databases and are stated in section 2. Further improvement in the performance is expected by selecting database specific parameters or the region of interest and can be attempted in further extension of this work.

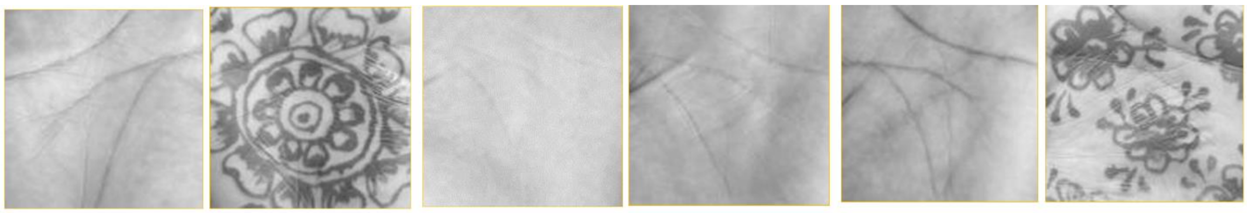

(a) Match score: 1.454 (b) Match score: 1.347 (c) Match score: 1.408

Figure 15: Sample palmprint image pairs from new database that failed to match. The first session images are shown on the left while *respective* second session images are shown on the right from the same hand/palm. All the three sets of images generated match scores higher than decision threshold (1.233) and therefore are considered as non-matched using the best performing method from this paper.

Automated and accurate segmentation of palmprint images, *i.e.* region of interest, is significantly important for the accurate matching of the palmprints. Accurate segmentation is quite challenging when images are acquired under contactless manner and further challenging when images are acquired under dynamic backgrounds. The segmentation accuracy of palmprint images can also alter the matching accuracy of palmprint images and the performance stated in this paper incorporated segmented images if/when they are made available with the database (*e.g.* IITD database [30] used for experiments in section 3.1). It is also worth noting that recent studies [34] have demonstrated that how the left hand palmprint images can themselves be used to match with the right hand palmprint images and thereby suggesting that strong correlation can exist between left and right palmprint images. This has been the key reason for preference for individually evaluating the palmprint matching performance from the two hands in this paper. Figure 15 illustrates few palmprint image samples from the two-session part of the database that failed to match. It can be observed from the image samples in figure 15 (a) and (c) that the second-session palm image samples are highly occluded due to the cosmetics. Accurate matching of such palmprint images requires the development of specialized algorithms to eliminate cosmetics and recover palmprint texture details for the matching and is suggested for the further work. New database introduced in this paper is acquired under varying illumination, *i.e.* ambient illumination, under indoor and outdoor environment. Therefore, despite best efforts in ensuring accurate segmentation of palmprint regions, there are few samples that are not accurately segmented. Figure 16 presents some image samples that represents such failure cases and underlines the need for further work in the development of accurate palmprint segmentation algorithms. It can be observed from these samples that the segmented region of interest is not correctly (at fixed relative distance from the normal to the key reference points) localized. These poorly segmented image samples however do not necessarily reflect the limitation of the segmentation algorithm but in many cases the key reason is the failure to correctly present hand images by the subject during contactless imaging, *e.g*., the first image sample in Figure 16 is from subject no. 111 and in this *particular* sample the subject has raised his/her hand with pose that is not along the *x-y* plane of the camera. The database introduced in this paper has been acquired from working population in more realistic environment and introduces new challenges for the researchers. Automated detection of the palm injury regions, detection and removal of cosmetic patterns, dirt or handwritten texts, can help to further improve the performance for matching such images and should be pursued in further work to advance contactless palmprint based personal identification.

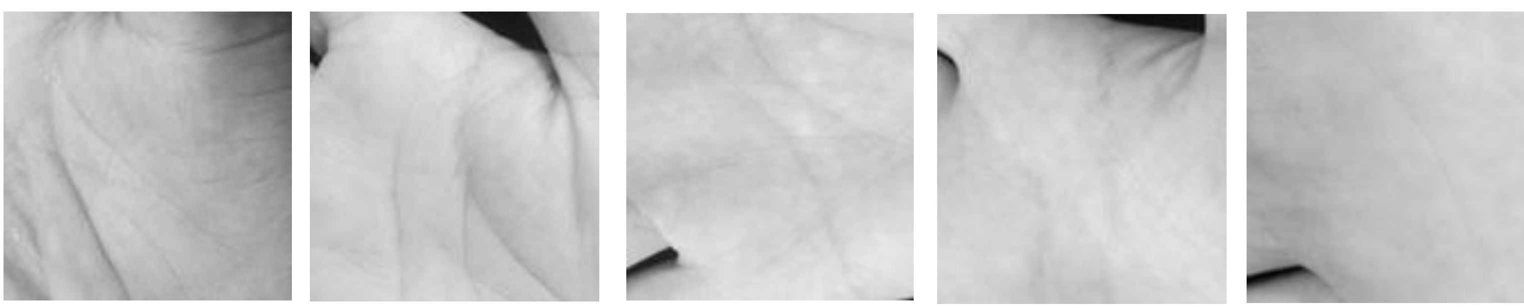

Figure 16: Sample palmprint images from new contactless database that were not adequately segmented.

Reference [36] has recently introduced a new contactless palmprint database and was accessed during the review process to ascertain the performance using the method introduced in this paper. The experimental protocol was to match second session images with the first session images. This generated 3,000 (300 × 10) genuine scores and 897,000 (10 × 300 × 299) impostor scores for each of the left and right palmprint images. The distribution of genuine and impostor match scores, for each of the left and right hand palmprint images, is shown in figure 17. It can be observed from this figure that the genuine and impostor match scores for the left and right palmprints are completely separated. The average genuine match score is 0.5369 while the range of genuine match scores is [0.2819 1.0124]. Similarly the average impostor match score is 1.3174 while the range of impostor match scores is [1.0601 1.5410]. Therefore, any decision threshold chosen between1.0124 to 1.0601 can offer perfect separation between the genuine and impostor scores. Therefore, the EER is 0% and the ROC is simply the straight line, for both the left and right cases. The reason for such performance can be attributed to very good quality palmprint images acquired by authors [35] under controlled illumination with a large imaging system, in addition to the capability of method introduced in section 2 to accommodate contactless imaging variations.

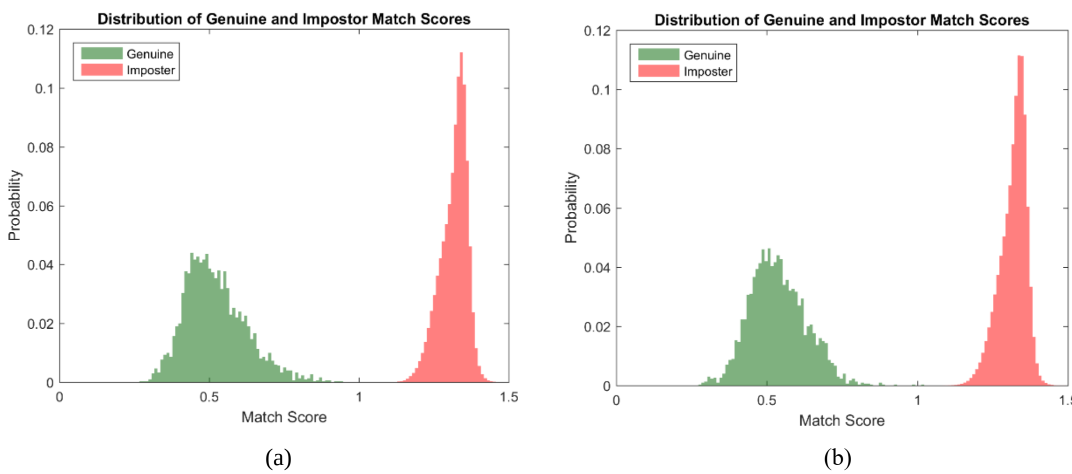

Figure 17: Distribution of genuine and impostor match scores for two session (a) left hand and (b) right hand pamprint images from additional experiments using the database in [36].

5. Conclusions and Further Work

Contactless palmprint identification offers promising solution to the hygiene and skin deformation problems. However, the contactless palmprint imaging generates relatively higher intra-class variations in successive images from the same subjects. Accurate matching of such palmprint images requires additional capabilities to robustly incorporate deformations along the camera axes.

This paper has investigated a new approach to match contactless palmprint images. The experimental results detailed in section of this paper on three publicly available database indicate outperforming results and validates the matching approach considered in this paper. Merit of contactless palmprint matching methods can be better-ascertained using results from the datasets with large population and variations. Therefore it is worth noting that the performance improvement from the approach investigated in this paper is significant for matching contactless palmprint images from the challenging and larger databases (*e.g*. ROC in figure 7 or ROC in figure 10). The results in section 2 also demonstrate 68.65% improvement in EER and 30.33% improvement in EER for these respective datasets. This paper has also presented a new contactless palmprint database in public domain. This database has been acquired from 600 different subjects, which is largest to-date, and includes images acquired under ambient illumination that can closely represent more user-friendly scenarios in future deployments. Earlier research on the palmprint identification and available databases have largely been focused on the palm images from subjects that represents office workers. The availability of database from diverse population that includes manual laborers, countryside school students, or hands from special capabilities, injury and cosmetics, will help to develop new solutions for the applicability of contactless palmprint technologies in new domains. Unlike any other known public palmprint databases, this database also provides images acquired from same subjects after long interval, *i.e.*, over 15 years, which can enable new insights on the stability of palmprint patterns. Availability of such images in public domain can also help to develop convincing courtroom arguments for the prosecution of suspects using forensic images where only the palmprint is the available piece of evidence.

Despite insightful details from the palmprint samples encountered from diverse populations and encouraging experimental results on this new database, the experiments reported in this paper should be considered preliminary. There are several limitations on the usage of the new database or for the contactless palmprint matching approach introduced in this paper. More experiments need to be done to utilize color information available in the palmprint images, to dynamically exploit larger palmprint area or on the development of algorithms that can detect (also correct) palm cosmetics, injury, or text to enable higher accuracy. Further work also needs to be done to evaluate the matching accuracy under more challenging matching protocols, *e.g*. combining left and right palms and for the left hand part of two-session database, and to reduce the computational complexity as the complexity of method introduced in this work is significantly higher than the baseline method in [9]. A multi-session palmprint database from large number of subjects, instead of two-session from this paper, is highly desirable to evaluate gradual temporal variations and should be developed in further extension of this work. In this work the focus has been on the authentication experiments and evaluating recognition accuracy in such large population can reveal strengths and weakness of various algorithms and is suggested for further work.

References

[1] D. Zhang, W. Zuo, and F. Yue, "A comparative study of palmprint recognition algorithms," *ACM Comput. Surv*., vol. 44, no. 1, pp 21–37, Jan. 2012.

[2] A. Kong, D. Zhang and M. Kamel, "A survey of palmprint recognition," *Pattern Recognition*, vol. 42, no. 7, pp. 1408-1418, 2009.

[3] A. Kumar and D. Zhang, "Personal recognition using hand-shape and texture," *IEEE Trans. Image Process*., vol. 15, no. 8, pp. 2454-2461, Aug. 2006,

[4] KTU Contactless Palmprint Database. [Online]. Available: http://ceng2.ktu.edu.tr/cvpr/contactlessPalmDB.htm.

[5] S. Ribaric and I. Fratric, "A Biometric identification system based on eigenpalm and eigenfinger Features", *IEEE Trans. Pattern Anal. Mach. Intell.*, vol. 27, no. 11, Nov. 2005.

[6] M. Choraś and Rafał Kozik, "Contactless palmprint and knuckle biometrics for mobile devices," *Pattern Analysis & Applications*, vol. 1, no. 15, 2012.

[7] V. Roux, S. Aoyama, K. Ito, T. Aoki, "Performance improvement of phase-based correspondence matching for palmprint recognition," *Proc. CVPR 2014 Biometrics Workshop*, CVPRW'14, pp. 70-77, 2014.

[8] A. W. K. Kong and D. Zhang, "Competitive coding scheme for palmprint verification", *Proc. 17th ICPR*, Washington, DC, pp. 1051-4651, 2004.

[9] Q. Zheng, A. Kumar, G. Pang, "A 3D feature descriptor recovered from a single 2D palmprint image," *IEEE Trans. Pattern Anal. Mach. Intell.*, vol. 38, pp. 1272-1279, June 2016.

[10] Z. Sun, T. Tan, Y. Wang, and S. Z. Li, "Ordinal palmprint representation for personal identification," *Proc. CVPR 2005*. pp. 279–284, 2005.

[11] K. O. Michael, T. Connie, and A. B. J. Teoh, "Touch-less palm print biometrics: novel design and implementation," *Image and Vis. Comput.*, vol. 26, no. 12, pp. 1551–1560, Dec. 2008.

[12] A. Morales, M. A. Ferrer, C. M. Travieso, and J. B. Alonso, “Multisampling approach applied to contactless hand biometrics,” *Proc. IEEE Int. Carnahan Conf. Security Technology*, pp. 224–229, 2012.

[13] A. Morales, M. A. Ferrer, and A. Kumar, “Towards contactless palmprint authentication,” *IET Vis. & Comput.*, vol. 5, no. 6, pp. 407–416, Nov. 2011.

[14] Q. Zhao, W. Bu, and X. Wu, “SIFT-based image alignment for contactless palmprint verification,” *Proc. IEEE Int. Conf. Biometrics*, ICB 2013, Madrid, Spain, 2013.

[15] L Li Liu, D Zhang, A Kumar, X Wu, “Tongue line extraction,” *Proc. 19th Intl. Conf. Pattern Recognition*, ICPR 2008, Tampa, Florida, 2008.

[16] M. Ekinci and M. Aykut, “Kernel Fisher discriminant analysis of Gabor features for online palmprint verification,” *Turk. J. Electr. Eng. Comput. Sci*., vol. 24, no. 2, pp. 355–369, Jan. 2016.

[17] GPDS100 Contactless Hands 2Band Database. [Online]. Available: http://www.gpds.ulpgc.es/download

[18] K. Ito, T. Aoki, H. Nakajima, K. Kobayashi, T. Higuchi, “A palmprint recognition algorithm using phase-only correlation,” *IEICE Trans. Fundamentals of Electronics, Communications and Computer Sciences*, vol. E91-A, pp. 1023-1030, April 2008.

[19] D. Zhang, W.-K. Kong, J. You, and M. Wong, “Online palmprint identification,” *IEEE Trans. Pattern Anal. Mach. Intell.*, vol.25, pp.1041-1050, Sep. 2003.

[20] W. Jia, D.-S. Huang, D. Zhang, “Palmprint verification based on robust line orientation code,” *Pattern Recognition*, vol. 41, pp. 1504-1513, May 2008

[21] X. Wu, K. Wang, and D. Zhang. "Palmprint texture analysis using derivative of Gaussian filters." *Proc. IEEE Intl. Conf. Comp. Intelligence and Security*, pp. 751-754, Nov. 2006.

[22] E.D. Castro, C. Morandi, “Registration of translated and rotated images using finite Fourier transform”, *IEEE Trans. Pattern Anal. Mach. Intell.*, vol. 9, pp.700-703, 1987.

[23] *PolyU-IITD Contactless Palmprint Database*, available at http://www.comp.polyu.edu.hk/~csajaykr/palmprint3.htm, 2017

[24] A. Kumar and Q. Zheng, “A method and device for contactless biometrics identification,” *Pending U. S. Patent No. 62032528*, Aug. 2014.

[25] Y. Zhou and A. Kumar, “Human identification using palm-vein images,” *IEEE Trans. Info. Forensics & Security*, vol. 6, no. 4, pp. 1159-1274, Dec. 2011

[26] K. Ito, T. Aoki, and S. Iitsuka, “A palmprint recognition algorithm using phase-based correspondence matching,” *Proc. Int’l Conf. Image Processing*, ICIP 2009, pp. 1977-1980, Nov. 2009.

[27] K. Takita, M.A. Muquit, T. Aoki, and T. Higuchi. A sub-pixel correspondence search technique for computer vision applications. *IEICE Trans. Fundamentals*, vol. E87-A, no. 8, pp. 1913-1923, Aug. 2004.

[28] PolyU Palmprint Palmprint Database. Available online from

http://www.comp.polyu.edu.hk/~biometrics, 2013.

[29] D. G. Lowe, “Distinctive image features from scale-invariant keypoints,” *Int. J. Computer Vision*, vol. 6, pp. 91–110, 2010.

[30] IITD Touchless Palmprint Database (Ver 1.0), *Available online*

http://www.comp.polyu.edu.hk/~csajaykr/IITD/Database_Palm.htm, Jan. 2014.

[31] CASIA Palmprint Database, *Available online from*: http://www.cbsr.ia.ac.cn/PalmDatabase.htm, 2016.

[32] C. Methani and A. Namboodiri, "Video based palmprint recognition," *Proc. ICPR 2010*, pp. 1352-1355, Istanbul, Turkey, 2010.

[33] H. Foroosh, J. B. Zerubia, and M. Berthod, "Extension of phase correlation to subpixel registration," *IEEE Trans. Image Processing*, vol. 11, pp. 188–200, Mar. 2002.

[34] A. Kumar and K. Wang, "Identifying humans by matching their left palmprint with right palmprint images using convolutional neural network," *Proc. First Intl. Workshop on Deep Learning and Pattern Recognition*, DLPR 2016, pp. 1-6, Cancun, Mexico, Dec. 2016.

[35] Q. Zheng, A. Kumar and G. Pan, "Suspecting less and achieving more: new insights on palmprint identification for faster and more accurate palmprint matching," *IEEE Trans. Info. Forensics & Security*, vol. 11, pp. 633-641, Mar. 2016

[36] L. Zhang, L. Li, A. Yang, Y. Shen, and M. Yang, "Towards contactless palmprint recognition: a novel device, a new benchmark, and a collaborative representation based identification approach," *Pattern Recognition*, vol. 69, pp. 199-212, 2017.